Chemical Science

EDGE ARTICLE

Realizing luminescent single crystals of covalent organic polymers with color-tunable emission through isomer engineering

Yanyan Qin,[abc] Pengfei She,*[abc] Xiaoda Wang,[ac] Jianjun Wu,[ac] Mingbing Lian,[ac] Feiyang Li, [ID][d] Shujuan Liu,[c] Qianfeng Gu, [ID][b] Yun Ma, [ID]*[ac] Qiang Zhao*[ac] and Qichun Zhang [ID]*[be]

Preparing luminescent single crystals of B–N-containing covalent organic polymers (COPs) is very important but highly challenging, since most conditions only produce luminescence-silent crystals. To address this issue, we employ an isomer engineering strategy to successfully prepare luminescent (**CityU-50**) and luminescence-silent (**CityU-60**) single crystals of B–N linked COPs based on two distinct chromophore isomers, 3,3′,6,6′-tetra(pyridin-4-yl)-9,9′-bicarbazole (3,6-TPy-BCz) and 2,2′,7,7′-tetra (pyridin-4-yl)-9,9′-bicarbazole (2,7-TPy-BCz). Single-crystal X-ray diffraction analysis reveals that 3,6-TPy-BCz can lead to a "loose" stacking model of helical polymer chains in **CityU-50**, effectively suppressing interchain aggregation and endowing **CityU-50** with unprecedented visible-light-excitable luminescence, while 2,7-TPy-BCz results in a "close" packing model of helical polymer chains in **CityU-60**, leading to a non-emissive structure. This factor validates our design principle. We also find that **CityU-50** can display excitation-dependent and solvent-responsive luminescence due to the different aggregation states within the crystal and solvent-triggered packing changes in the polymer chains of **CityU-50**. Based on these responses, we demonstrate the application of **CityU-50** in advanced information encryption. This work not only delivers a new class of smart crystalline materials but also establishes a powerful strategy for engineering crystalline polymers with precisely tailored structures and properties.

Introduction

Photoluminescent (PL) organic single crystals have drawn great attention benefiting from their potential applications in cutting-edge technologies such as optical waveguides, optical communication, displays and advanced information encryption.[1–5] However, it is a challenge to obtain luminescent single crystals of covalent organic polymers/frameworks (COPs/COFs) because of the aggregation-caused quenching (ACQ) effect, a common phenomenon in conjugated polymers, and

[a]College of Electronic and Optical Engineering and College of Flexible Electronics (Future Technology), Nanjing University of Posts and Telecommunications, Nanjing 210023, P. R. China. E-mail: pengfei.she@njupt.edu.cn; iamyma@njupt.edu.cn; iamqzhao@nuist.edu.cn

[b]Department of Materials Science and Engineering, City University of Hong Kong, Tat Chee Avenue, Kowloon Tong, Hong Kong, P. R. China. E-mail: qiczhang@cityu.edu.hk

[c]State Key Laboratory of Flexible Electronics (LoFE), Institute of Advanced Materials (IAM), Nanjing University of Posts and Telecommunications, Nanjing 210023, P. R. China

[d]School of Environmental and Chemical Engineering, Jiangsu University of Science and Technology, Zhenjiang 212100, P. R. China

[e]City University of Hong Kong Shenzhen Research Institute Shenzhen, Guangdong Province, 518057, P. R. China

the inherent synthetic difficulties in growing long-range crystalline order with desired functionalities.[6–8] To elucidate the underlying PL quenching mechanism, growing luminescent single crystals of COPs for single-crystal X-ray diffraction (SCXRD) analysis is extremely necessary because this technique enables the accurate identification of geometric factors such as atomic positions, bond lengths and angles, stacking patterns and crucial host-guest molecular interactions.[9–12] Importantly, the detailed structural information not only helps to understand the growing kinetics and thermodynamics of single crystals but also offers a well-established platform to elucidate the relationships among building blocks, structures, and luminescent properties.

Currently, highly reversible covalent bonds, such as imine linkages, boron ester linkages and dative B–N bonds, have been extensively utilized to grow single crystals of COPs by facilitating efficient self-correction of defects during the self-assembly process.[13–20] Compared to imine (∼600 kJ mol^{-1}) and boronate ester (∼500 kJ mol^{-1}) bonds, dative B–N bonds possess relatively low binding energy (approximately 100 kJ mol^{-1}). This lower energy facilitates the formation of large single crystals through reversible self-assembly. Although a series of large single crystals of functional COPs featuring B–N bonds have
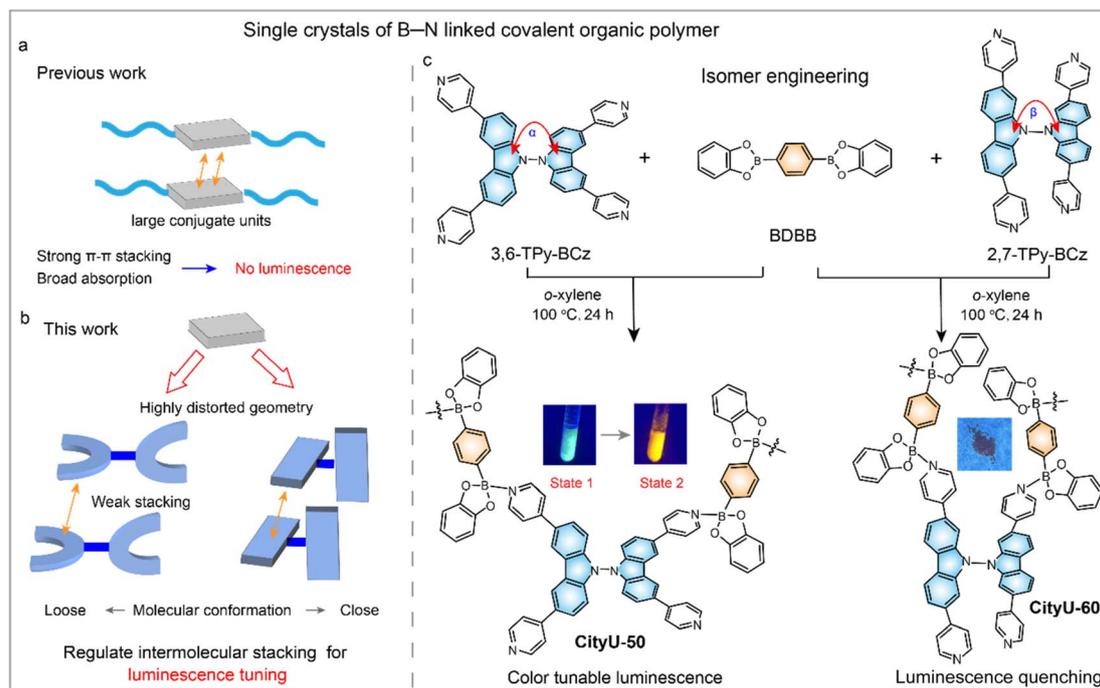
Fig. 1 Schematic illustration of the design strategy for luminescent COPs. (a and b) Schematic design of distorted building units with loose and close conformations, regulating intermolecular stacking of COPs for luminescence tuning. (c) Synthetic routes to **CityU-50** and **CityU-60**. The left insets are photographs of **CityU-50** before and after treatment with *n*-hexane under UV and visible light. State 1 refers to **CityU-50** crystals without any treatment, while State 2 refers to **CityU-50** crystals that were soaked in *n*-hexane at room temperature for 1 h. The right inset is a photograph of **CityU-60** under UV or visible light.

been extensively reported, the luminescence properties remain scarcely mentioned (Fig. 1a).[21–32] Besides, developing stimuli-responsive luminescent COPs that are capable of dynamically modulating their emission properties in response to external stimuli is particularly interesting for next-generation photonic applications, notably in anti-counterfeiting technologies.[33,34]

Here, we address this long-standing issue by proposing an isomer engineering strategy. We designed two highly distorted chromophore isomers, a "loose" 3,3′,6,6′-tetra(pyridin-4-yl)-9,9′-bicarbazole (3,6-TPy-BCz) and a "close" 2,2′,7,7′-tetra(pyridin-4-yl)-9,9′-bicarbazole (2,7-TPy-BCz). We hypothesized that the sterically bulky, loose conformation of 3,6-TPy-BCz would effectively disrupt intermolecular π-π stacking to overcome ACQ, while simultaneously creating sufficient free volume to accommodate external stimuli (Fig. 1b). Then, two single crystals of B–N linked COPs (luminescent **CityU-50** and non-emissive **CityU-60**) were prepared using chromophore isomers and 1,4-bis(benzo[*d*][1,2,3]dioxaborol-2-yl)benzene (BDBB) as building units (Fig. 1c). As expected, **CityU-50** exhibits significant visible-light-excitable green emission, while **CityU-60** is completely non-emissive. SCXRD analysis reveals that the persistence of a solvent sheath of six *o*-xylene molecules encapsulating each unit in **CityU-50** effectively isolates the polymer chains and impedes detrimental interchain π–π stacking. In contrast, in its "close" isomer-based counterpart (**CityU-60**), many π–π interactions exist between adjacent polymer chains, perfectly validating our design principle. Interestingly, **CityU-50** displays excitation-dependent and

solvent-responsive luminescence behaviors. Based on the feature of color-tunable luminescence in **CityU-50**, we demonstrate its application in advanced information encryption. This work not only delivers a new class of functional crystalline materials but also establishes a powerful design strategy for engineering smart luminescent polymers with precisely tailored structures and properties.

Results and discussion

The single crystals of **CityU-50** and **CityU-60** were firstly prepared using distinct chromophore isomers (3,6-TPy-BCz and 2,7-TPy-BCz) and BDBB as building blocks under solvothermal conditions. Briefly, 3,6-TPy-BCz or 2,7-TPy-BCz and BDBB (molar ratio = 1 : 1) were mixed in dry *o*-xylene and heated at 100 °C for 24 hours. After cooling to room temperature, large colorless single crystals (up to 5 mm) of **CityU-50** were formed at the bottom of the reaction vessel, whereas small faint yellow single crystals (up to 3 mm) of **CityU-60** were found. The synthesis procedure is illustrated in Fig. 1c. The detailed experimental process as well as the characterization data are provided in the SI (Scheme S1 and Fig. S1–S6).

To elucidate the impact of isomer engineering on structural characteristics, SCXRD analysis of **CityU-50** and **CityU-60** was conducted. The data analysis reveals that **CityU-50** crystallizes in the monoclinic *C*2/*c* space group with lattice constants of $a = 24.5308(4)$ Å, $b = 10.3508(2)$ Å, and $c = 31.7355(6)$ Å, and a unit-cell volume of 7507.2(3) Å^3 (Table S1). The asymmetric unit of

CityU-50 consists of one 3,6-TPy-BCz moiety, two half BDBB species, and two *o*-xylene molecules (Fig. S7a). Notably, within the 3,6-TPy-BCz building block, four pyridine rings exhibit a significantly twisted arrangement, characterized by dihedral angles of 27.50 and 10.98° (Fig. S7b). The dihedral angles of two carbazole planes and bond lengths of N–N between two carbazole planes are 89.43° and 1.38 Å, respectively. Further analysis reveals that one 3,6-TPy-BCz unit connects two BDBB species *via* dative B–N bonds with a B–N bond length of 1.66 Å, forming 1D helical chains with a helical pitch of 25.21 Å along the *c*-axis (Fig. 2a). This helical architecture, arising from the twisted 3,6-TPy-BCz units and B–N linkages, inherently creates an internal free volume within the COP chains. This helical architecture enforces a remarkable separation between the chromophores, with the distance between adjacent 3,6-TPy-BCz units along the *c*-axis reaching 31.74 Å. Importantly, this separation is maintained by a solvent sheath of six *o*-xylene molecules encapsulating each unit, which could contribute to isolating the polymer chains and impeding detrimental interchain π–π stacking. On the other hand, SCXRD measurement reveals that **CityU-60** adopts a monoclinic $P2_1/n$ space group with lattice constants of $a = 16.4184(2)$ Å, $b = 17.0819(2)$ Å, and $c = 21.1989(2)$ Å, and a unit-cell volume of 5687.75(11) Å^3 (Table S2). The asymmetric unit of **CityU-60** consists of one 2,7-TPy-BCz moiety, one BDBB species, and one *o*-xylene molecule. Unlike **CityU-50**, **CityU-60** exhibits a markedly smaller dihedral angle of 74.73° between its two carbazole planes (Fig. S8), indicating that

its more compact geometry is predicted to favor aggregation. Indeed, SCXRD analysis of **CityU-60** reveals a dramatically different packing motif. Instead of isolated helical chains, **CityU-60** forms compact, 1D wave-like chains (Fig. 2b). This conformation drastically reduces the inter-chromophore distance along the *c*-axis to 17.08 Å, nearly half that of **CityU-50**.

Furthermore, the space arrangements of **CityU-50** and **CityU-60** also exhibit a significant difference. For **CityU-50**, the coordinated pyridine rings and carbazole planes within a single chain allow the formation of tight π–π interactions with adjacent *o*-xylene rings with short distances of 3.99 Å and 3.80 Å, respectively (Fig. 3a and b). These π–π interactions, mediated by *o*-xylene molecules, can bridge adjacent helical chains, contributing to the formation of a pseudo-2D layer. In addition, the C–H⋯π interactions between the benzene rings from BDBB within a single chain and free pyridine molecules in adjacent chains further stabilize this pseudo-2D layer. The presence of solvent molecules within the crystal lattice also suggests potential for solvent-responsive behavior. Moreover, the pseudo-2D layers are interconnected through C–H⋯O interactions between the oxygen atoms of B-aryl rings and *o*-xylene molecules, as well as C–H⋯C interactions between adjacent *o*-xylene molecules, resulting in the formation of a supramolecular architecture (Fig. S9). Remarkably, no π–π interaction between adjacent polymer chains is found in the crystals of **CityU-50** (Fig. 3c). Unlike the solvent-mediated assembly in **CityU-50**, the pseudo-2D layers in **CityU-60** are formed through
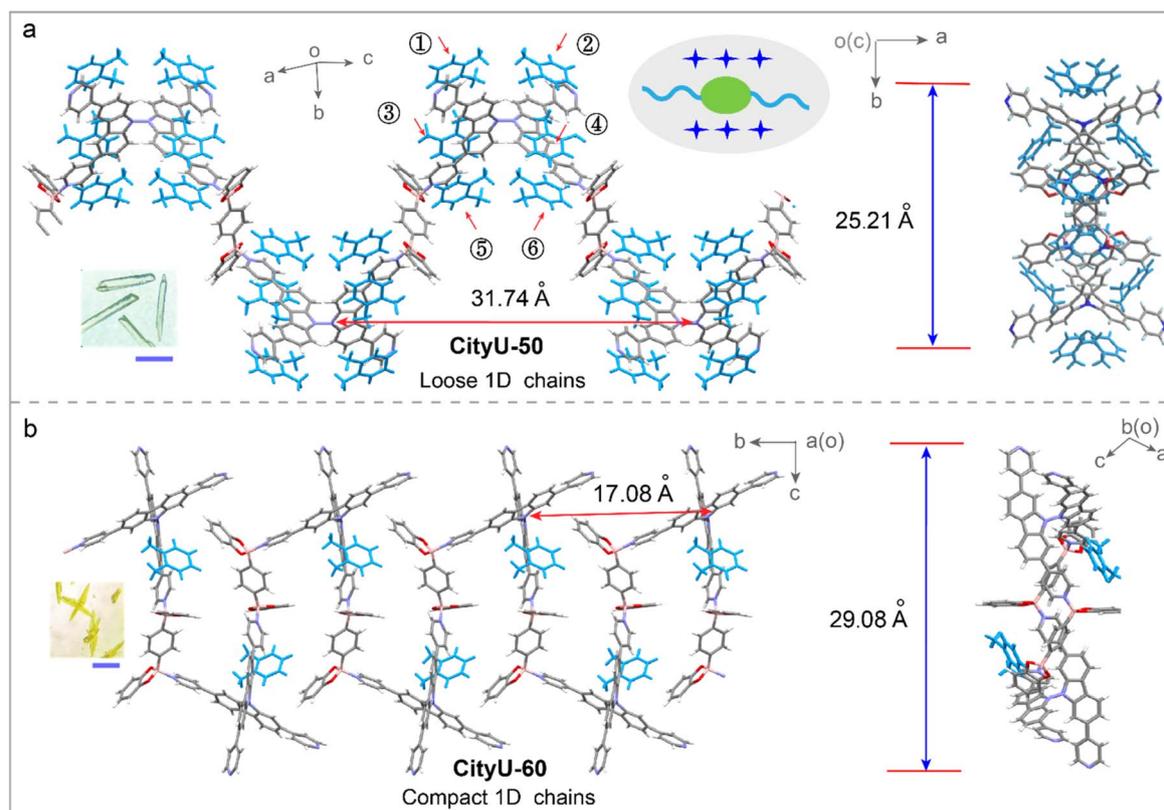

Fig. 2 The 1D chains of **CityU-50** (a) and **CityU-60** (b). Inset: photos of single crystals of **CityU-50** and **CityU-60**. Scale bar = 3 mm.
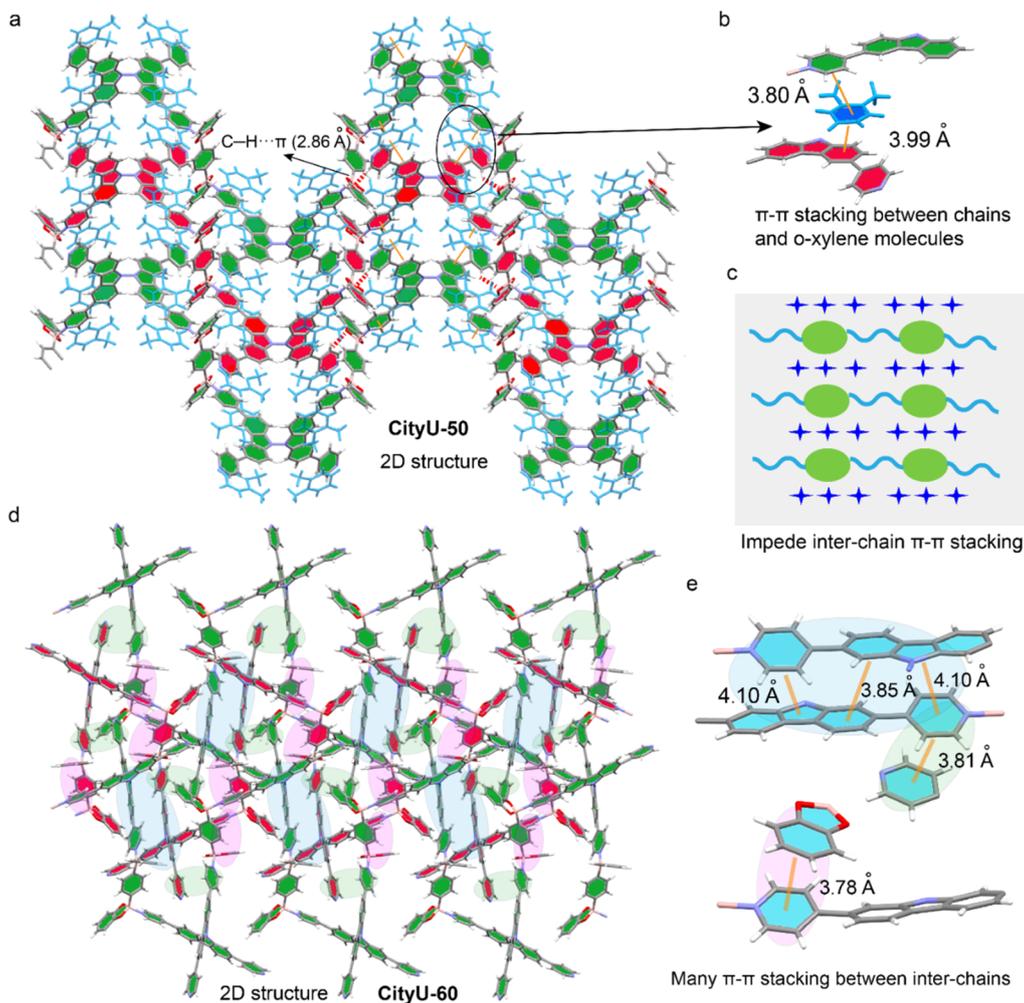
Fig. 3 The 2D structures and stacking modes of **CityU-50** (a–c) and **CityU-60** (d and e).

extensive, direct π–π interactions (3.78–4.10 Å) among BDBB, pyridine rings and carbazole planes in adjacent polymer chains (Fig. 3d and e). Furthermore, independent gradient model (IGM) analysis confirms this stark difference, visualizing widespread π–π interactions between pyridine and carbazole moieties in **CityU-60**, which are conspicuously absent in **CityU-50** (Fig. S10). Besides, the experimental powder X-ray diffraction (PXRD) results and the simulated patterns match each other well, indicating that the as-synthesized **CityU-50** and **CityU-60** samples exhibit high phase purity (Fig. S11 and S12). Field-emission scanning electron microscopy (FESEM) analysis reveals that the **CityU-50** crystals possess a cubic-like 3D morphology (Fig. S13). Energy dispersive spectroscopy (EDS) mapping confirms the existence of oxygen, nitrogen and boron elements in the B–N crystal. Besides, the porosities of **CityU-50** and **CityU-60** single crystals were further investigated *via* a nitrogen adsorption experiment at 77 K. The isotherms and pore size distribution curves, calculated by the Brunauer–Emmett–Teller (BET) and Barrett–Joyner–Halenda (BJH) methods, are presented in Fig. S14. **CityU-50** possesses a small BET surface area of 4.51 m^2 g^{-1}, along with a pore volume of

0.0092 cm^3 g^{-1}, while the **CityU-60** exhibits a BET surface area of 7.13 m^2 g^{-1} and pore volume of 0.016 cm^3 g^{-1}, suggesting that both polymers are virtually nonporous. Thus, we believe that this profound structural discrepancy between **CityU-50** and **CityU-60** should directly affect their optical properties due to a possible ACQ effect.

To validate our hypothesis, the photoluminescence (PL) properties of **CityU-50** and **CityU-60** samples were investigated. Excitingly, **CityU-50** exhibits intense green emission under 365 nm UV irradiation, with the primary emission peak at ~535 nm (Fig. 4a). Meanwhile, the 3,6-TPy-BCz monomer displays a significantly blue-shifted emission peak at 385 nm, thereby excluding the possibility that the green emission originates from the 3,6-TPy-BCz monomer (Fig. S15). The photoluminescence quantum yield (PLQY) and lifetime at 535 nm are measured to be 4.43% and 7.8 ns (Fig. 4b), respectively, confirming its fluorescence feature. From the excitation-luminescence mapping of **CityU-50** (Fig. 4c), it is evident that the optimized excitation wavelength is 435 nm, indicating that the green emission from **CityU-50** can be efficiently triggered by a visible light source. In contrast, a complete shutdown of
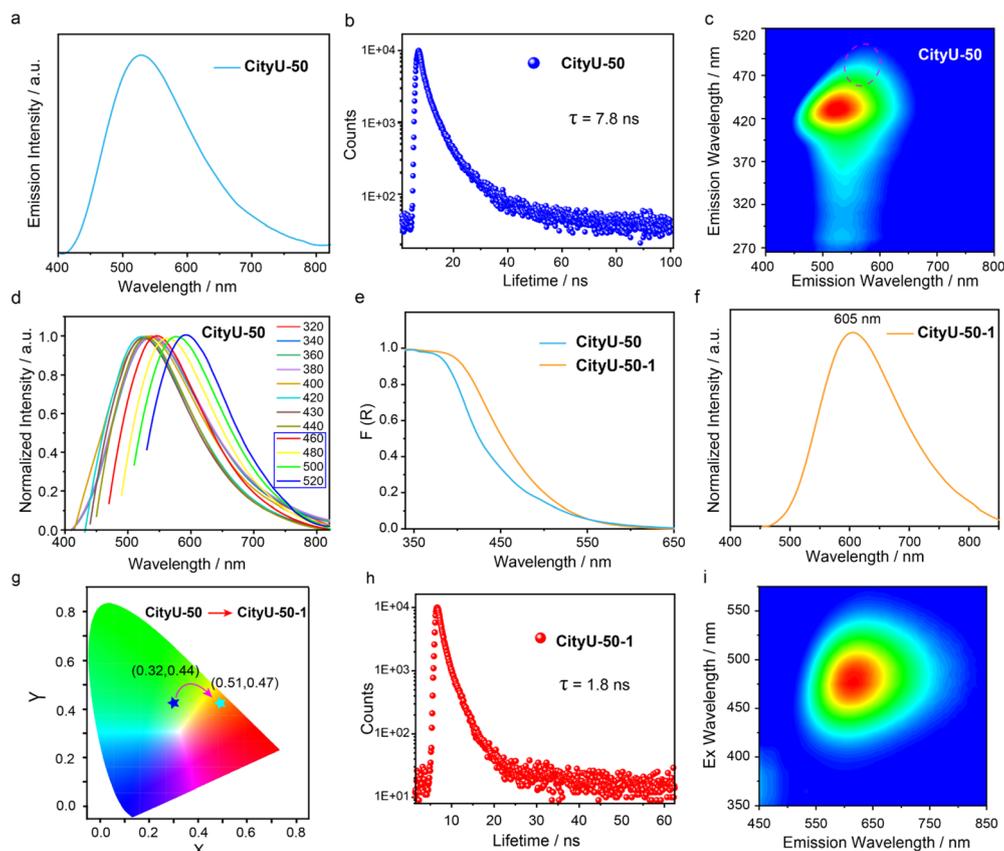
Fig. 4 The photoluminescent properties of **CityU-50** and **CityU-50-1** (**CityU-50** after treatment with *n*-hexane). (a) Photoluminescence, (b) lifetime decay profiles (535 nm), (c) mapping of excitation-photoluminescence and (d) excitation-dependent photoluminescence of **CityU-50**, recorded under ambient conditions at 298 K. (e) UV-Vis diffuse reflectance spectra of **CityU-50** and **CityU-50-1** converted using the Kubelka–Munk function, F(R). (g) CIE coordinate diagram of **CityU-50** and **CityU-50-1**. (f) Photoluminescence, (h) lifetime decay profiles (605 nm) and (i) mapping of excitation-photoluminescence of **CityU-50-1**, recorded under ambient conditions at 298 K.

optical emission is observed in **CityU-60** sample (Fig. S16), indicating that suppressing interchain stacking is key to luminescence. Meanwhile, this stark, "lights-off" result in **CityU-60**, when contrasted with the bright, tunable emission of **CityU-50**, provides unambiguous evidence that the isomer molecular conformation of the building block directly governs the packing of polymers, which in turn dictates its luminescent properties. Interestingly, it is found that the **CityU-50** sample exhibits the obviously color tunable luminescence feature upon multiple external stimuli. As shown in Fig. 4d and S17, different from excitation wavelengths ranging from 320 to 440 nm, **CityU-50** exhibits excitation-dependent PL behavior within the range of 440–520 nm. Specifically, **CityU-50** displays an orange emission peak at 595 nm when excited at 520 nm. This excitation-dependent luminescence may likely originate from distinct emissive species associated with different aggregation states within the crystal,[35–37] generated by crystal defects stemming from the loss of *o*-xylene. Therefore, the dominant green emission of the **CityU-50** sample may also be fully modified to dominant orange emission by the exchange or removal of *o*-xylene. To confirm this guess, **CityU-50** crystals were soaked in *n*-hexane at room temperature for 1 h, and the corresponding solid-state absorption and PL spectra were recorded. The

sample treated with *n*-hexane is referred to as **CityU-50-1**. As depicted in Fig. 4e, **CityU-50-1** exhibits a distinct redshift in its absorption spectrum compared to **CityU-50**, suggesting a potential alteration in the electronic transitions resulting from changes in either molecular structure or intermolecular stacking arrangements. Importantly, a notable redshift in the luminescence spectra is observed, with the main emission peak shifting from 535 nm to 605 nm (Fig. 4f). This spectral shift is accompanied by a change in emission color from green to orange, with the corresponding CIE coordinates shifting from (0.32, 0.44) to (0.51, 0.47) (Fig. 4g). Furthermore, the PLQY and lifetime at 605 nm of **CityU-50-1** are measured to be 5.58% and 1.8 ns, respectively (Fig. 4h). Unlike **CityU-50**, the luminescence of **CityU-50-1** can only be excited by visible light, and no obvious excitation-dependent luminescence behavior is observed (Fig. 4i and S18). This suggests that the solvent-induced structural change in **CityU-50-1** leads to a more homogeneous aggregation state, resulting in a single dominant emissive species and the elimination of excitation-dependent luminescence. To elucidate whether the exchange or removal of *o*-xylene in **CityU-50** induces this color-tunable luminescence, a series of control experiment were carried out. Firstly, the luminescence behavior of **CityU-50** was monitored in different solvents. It's

found that smaller solvent molecules more readily induce the luminescence color response (Fig. S19). Subsequently, Fourier-transform infrared spectra (FTIR) of **CityU-50** and **CityU-60** exhibit minimal variation, indicating that the chain structure of **CityU-50** remains essentially intact after *n*-hexane exposure (Fig. S20). Time-dependent PXRD measurements on **CityU-50** soaked in *n*-hexane for different durations were carried out. As shown in Fig. S21, with increasing soaking time, broad bands gradually appear in the range of 15–30°. Moreover, the original diffraction peaks remain discernible even after prolonged *n*-hexane exposure. These results indicate that prolonged exposure to *n*-hexane leads to the gradual collapse of the molecular stacking of **CityU-50**. Furthermore, we attempted to directly remove *o*-xylene solvent molecules from single crystals of **CityU-50** by heating and subsequently investigate the photophysical properties. After heating single crystals of **CityU-50** at 150 °C for 1 h, we found that the PXRD pattern, absorption, and luminescence of the sample are similar to those observed after *n*-hexane treatment (**CityU-50-1**), rather than those of the as-synthesized **CityU-50** (Fig. S22 and S23). Furthermore, we conducted time-dependent density functional theory (TDDFT) calculations on monomer and dimer fragments. The results show that dimer fragments exhibit a lower energy level in the excited singlet state relative to the monomer (Fig. S24). Thus, the above-mentioned results clearly demonstrate that the unique solvent-responsive luminescence behavior of **CityU-50** can be attributed to the aggregation of polymer chains within the crystal structure, triggered by the exchange and removal of *o*-xylene molecules, which induces a change in intermolecular packing and enhances intermolecular interactions. Meanwhile, the excitation-dependent luminescence behavior of **CityU-50** should be attributed to the presence of multiple aggregation states within the crystal lattice. These distinct aggregation states, potentially varying in their extent and influenced by factors such as crystal defects resulting from the partial loss of *o*-xylene molecules, could give rise to different emissive species, thus accounting for the observed excitation-dependent emission.

Given the distinctive color tunable luminescence behaviors of **CityU-50**, we exploited its promising applications in anti-counterfeiting and optical information storage (Fig. 5a). As illustrated in Fig. 5b, the encryption digit "8" was prepared using **CityU-50** microcrystals. Initially, under 365 nm UV light illumination, the digit "8" exhibits a pronounced green emission. Subsequently, upon adding *n*-hexane to a part of the pattern, only the digit "1" remains visible (Fig. 5c). However, under 480 nm visible light illumination, the digit "8" with orange emission becomes discernible. This result highlights the outstanding potential of the tunable luminescent B–N polymer single crystals for advanced optical information storage and encryption applications.

Conclusions

In conclusion, by introducing two distorted chromophore isomers with different conformations as building units, we have demonstrated that loose and close conformations have a dramatic impact on the single-crystal structures and optical properties of COPs. SCXRD analysis shows that **CityU-50** with a loose conformation is a 1D helical polymer, where *o*-xylene solvent molecules play a critical role in directing the crystal packing and supramolecular architecture, while the dense packing and pervasive π–π interactions between adjacent 1D chains are found in the pseudo-2D layer of **CityU-60** with a close conformation. Consequently, **CityU-50** exhibits excitation-dependent and solvent-responsive luminescence. Comprehensive experimental and theoretical investigations indicate that the excitation-dependent luminescence arises from the presence of multiple aggregation states within the crystal lattice, and solvent-responsive luminescence is attributed to an aggregation of polymer chains, triggered by the exchange of lattice-confined *o*-xylene molecules. Based on this distinctive tunable luminescence, we have demonstrated its application in advanced information encryption and optical storage areas. Significantly, this work not only showcases the practical utility of **CityU-50** but also establishes a robust design principle for engineering stimulus-responsive luminescent crystalline polymers based on distorted chromophores and dynamic B–N linkages.

Author contributions

P. She, Y. Ma, Q. Zhao and Q. Zhang conceived the project and experiments. Y. Qin designed the molecules. Y. Qin and X. Wang conducted the experiment and wrote the manuscript. S. Liu helped revise the manuscript. J. Wu, M. Lian and Q. Gu performed the optical application. F. Li conducted the theoretical calculation. All authors contributed to writing the manuscript.

Conflicts of interest
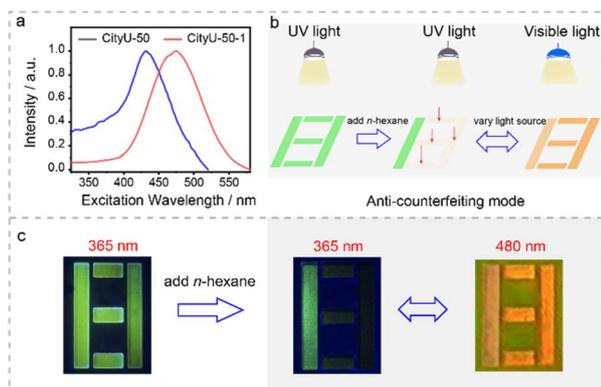
There are no conflicts to declare.

Fig. 5 Optical application. (a) Excitation spectra of **CityU-50** and **CityU-50-1** (**CityU-50** after treatment with *n*-hexane). (b and c) Visual representation illustrating the process of information encryption and decryption.

Data availability

CCDC 2414993 and 2465520 contain the supplementary crystallographic data for this paper.[38a,b]

The authors confirm that the data supporting the findings of this study are available within the article and its supplementary information (SI). Supplementary information: synthetic procedures, experimental details and supplemental figures. See DOI: https://doi.org/10.1039/d5sc09875k.

Acknowledgements

References

1 (a) X. Wang, Z. Wang, X. Wang, F. Kang, Q. Gu and Q. Zhang, *Angew. Chem., Int. Ed.*, 2024, **63**, e202416181; (b) D. Chen, Z. Chen, Y. Yang, Y. Wang, X. Han, K. Y. Lau, Z. Wu, C. Zou, Y. Zhang, B. Xu, X. Liu, Z. Ma, G. Dong, G. Barillaro, L. Zhong and J. Qiu, *Adv. Mater.*, 2024, **36**, 2404493; (c) S. Yang, Y. Li, F. Kang, F. Li, S. Zhao, Y. Sun, C. Zhang and Q. Zhang, *Adv. Funct. Mater.*, 2025, **35**, 2504976.

2 Z. Qin, Y. Zhang, T. Wang, H. Gao, C. Gao, X. Zhang, H. Dong and W. Hu, *Nat. Photonics*, 2025, **19**, 378–386.

3 L. Catalano, J. Berthaud, G. Dushaq, D. P. Karothu, R. Rezgui, M. Rasras, S. Ferlay, M. W. Hosseini and P. Naumov, *Adv. Funct. Mater.*, 2020, **30**, 2003443.

4 (a) S. Han, S. Zhu, G. Fan, X. Huang, G. Zhao, R. Shi, Y. Huang, M. Wu, J. Li, Y. Guo, Y. Gao, S. Zhuang, F. Cao, X. Yu and D. Zhang, *Adv. Funct. Mater.*, 2024, **35**, 2421770; (b) L. Xu, J. Zhang, L. Yin, X. Long, W. Zhang and Q. Zhang, *J. Mater. Chem. C*, 2020, **8**, 6342–6349; (c) P. Gu, Z. Wang and Q. Zhang, *J. Mater. Chem. B*, 2016, **4**, 7060–7074; (d) P. Gu, Y. Zhao, J. He, J. Zhang, C. Wang, Q. Xu, J. Lu, X. Sun and Q. Zhang, *J. Org. Chem.*, 2015, **80**, 3030–3035; (e) H. Ye, G. Liu, S. Liu, D. Casanova, X. Ye, X. Tao, Q. Zhang and Q. Xiong, *Angew. Chem., Int. Ed.*, 2018, **57**, 1928–1932; (f) Z. Wang, F. Yu, W. Chen, J. Wang, J. Liu, C.-j. Yao, J. Zhao, H. Dong, W. Hu and Q. Zhang, *Angew. Chem., Int. Ed.*, 2020, **59**, 17580–17586.

5 Y. Liu, G. Liu, Y. Wu, W. Cai, Y. Wang, S. Zhang, H. Zeng and X. Li, *Adv. Mater.*, 2023, **35**, 2301914.

6 S. Xu and Q. Zhang, *Mater. Today Energy*, 2021, **20**, 100635.

7 Y. Wang, Y.-Z. Cheng, K.-M. Wu, D.-H. Yang, X.-F. Liu, X. Ding and B.-H. Han, *Angew. Chem., Int. Ed.*, 2023, **62**, e202310794.

8 X. Sheng, Z. Wang, G. Sheng, C. Zhu, D. Xiao, T. Shan, X. Xiao, M. Liu, G. Li, Y. Zhu, J. L. Sessler and F. Huang, *J. Am. Chem. Soc.*, 2024, **146**, 12547–12555.

9 D. Beaudoin, T. Maris and J. D. Wuest, *Nat. Chem.*, 2013, **5**, 830–834.

10 F. Hu, W. Hao, D. Mücke, Q. Pan, Z. Li, H. Qi and Y. Zhao, *J. Am. Chem. Soc.*, 2021, **143**, 5636–5642.

11 P. Kissel, D. J. Murray, W. J. Wulftange, V. J. Catalano and B. T. King, *Nat. Chem.*, 2014, **6**, 774–778.

12 Q.-H. Guo, M. Jia, Z. Liu, Y. Qiu, H. Chen, D. Shen, X. Zhang, Q. Tu, M. R. Ryder, H. Li, P. Chen, Y. Xu, P. Li, Z. Chen, G. S. Shekhawat, V. P. Dravid, R. Q. Snurr, D. Philp, A. C. H. Sue, O. K. Farha, M. Rolandi and J. F. Stoddart, *J. Am. Chem. Soc.*, 2020, **142**, 6180–6187.

13 T. Ma, E. A. Kapustin, S. X. Yin, L. Liang, Z. Zhou, J. Niu, L.-H. Li, Y. Wang, J. Su, J. Li, X. Wang, W. D. Wang, W. Wang, J. Sun and O. M. Yaghi, *Science*, 2018, **361**, 48–52.

14 A. M. Evans, L. R. Parent, N. C. Flanders, R. P. Bisbey, E. Vitaku, M. S. Kirschner, R. D. Schaller, L. X. Chen, N. C. Gianneschi and W. R. Dichtel, *Science*, 2018, **361**, 52–57.

15 X. Wang, M. Bahri, Z. Fu, M. A. Little, L. Liu, H. Niu, N. D. Browning, S. Y. Chong, L. Chen, J. W. Ward and A. I. Cooper, *J. Am. Chem. Soc.*, 2021, **143**, 15011–15016.

16 C. Gropp, T. Ma, N. Hanikel and O. M. Yaghi, *Science*, 2020, **370**, eabd6406.

17 J. Yang, F. Kang, X. Wang and Q. Zhang, *Mater. Horiz.*, 2022, **9**, 121–146.

18 T. Ma, L. Wei, L. Liang, S. Yin, L. Xu, J. Niu, H. Xue, X. Wang, J. Sun, Y.-B. Zhang and W. Wang, *Nat. Commun.*, 2020, **11**, 6128.

19 A. Natraj, W. Ji, J. Xin, I. Castano, D. W. Burke, A. M. Evans, M. J. Strauss, M. Ateia, L. S. Hamachi, N. C. Gianneschi, Z. A. Alothman, J. Sun, K. Yusuf and W. R. Dichtel, *J. Am. Chem. Soc.*, 2022, **144**, 19813–19824.

20 (a) L. He, T. Naren, L. Zhang, F. Kang, J. Yang, Z. Chen, A. Yu, D.-S. Li, L. Chen and Q. Zhang, *Angew. Chem., Int. Ed.*, 2025, **64**, e202506036; (b) N. Luisier, K. Bally, R. Scopelliti, F. T. Fadaei, K. Schenk, P. Pattison, E. Solari and K. Severin, *Cryst. Growth Des.*, 2016, **16**, 6600–6604; (c) M. Xue, L. Zhang, X.-X. Li, Z. Chen, F. Kang, X. Wang, Q. Dong, X. Wang, C.-S. Lee, Y.-Q. Lan and Q. Zhang, *Nat. Commun.*, 2024, **15**, 10026; (d) M. Xue, L. Zhang, X. Meng, J. Yang, Y. He, C.-S. Lee, J. Zhang and Q. Zhang, *Angew. Chem., Int. Ed.*, 2024, **63**, e202412289; (e) M. Xue, L. Zhang, X. Wang, Q. Dong, Z. Zhu, X. Wang, Q. Gu, F. Kang, X.-X. Li and Q. Zhang, *Angew. Chem., Int. Ed.*, 2024, **63**, e202315338; (f) M. Xue, J. Yang, F. Kang, X. Wang and Q. Zhang, *J. Mater. Chem. C*, 2022, **10**, 17027–17047; (g) M. Xue, G. Ye, L. Zhang, Q. Dong, C.-S. Lee, Z. Li and Q. Zhang, *Chem. Sci.*, 2025, **16**, 5260–5265.

21 X. Wang, Z. Ke, L. Liu, J. Huang, Y. Yang, W. Dai, C. Liu, Z. Zhang, Z. Yao and S. Xiang, *Cryst. Growth Des.*, 2021, **21**, 3168–3174.

22 T. Shan, L. Chen, D. Xiao, X. Xiao, J. Wang, X. Chen, Q.-H. Guo, G. Li, J. F. Stoddart and F. Huang, *Angew. Chem., Int. Ed.*, 2024, **63**, e202317947.

23 (*a*) X. Wang, L. Zhang, X. Wang, T. Cheng, M. Xue, M. Q. Dong, Y. Peng and Q. Zhang, *Adv. Func. Mater.*, 2024, **35**, 2401362; (*b*) Z. Chen, T. Naren, L. Zhang, J. Yang, Q. Gu, F. Kang, L. Chen and Q. Zhang, *Angew. Chem., Int. Ed.*, 2025, **64**, e202517238.

24 L. Zhang, Z. Chen, X.-X. Li, X. Wang, Q. Gu, X. Wang, C.-S. Lee, Y.-Q. Lan and Q. Zhang, *Angew. Chem., Int. Ed.*, 2024, **63**, e202411018.

25 J. Wang, W. You, L. Chen, D. Xiao, X. Xiao, T. Shan, Y. Liu, M. Liu, G. Li, W. Yu and F. Huang, *Angew. Chem., Int. Ed.*, 2024, **63**, e202405761.

26 W. Wang, L. Wang, F. Du, G.-D. Wang, L. Hou, Z. Zhu, B. Liu and Y.-Y. Wang, *Chem. Sci.*, 2023, **14**, 533–539.

27 X. Xiao, D. Xiao, G. Sheng, T. Shan, J. Wang, X. Miao, Y. Liu, G. Li, Y. Zhu, J. L. Sessler and F. Huang, *Sci. Adv.*, 2023, **9**, eadi1169.

28 Q. Dong, T. Naren, L. Zhang, W. Jiang, M. Xue, X. Wang, L. Chen, C.-S. Lee and Q. Zhang, *Angew. Chem., Int. Ed.*, 2024, **63**, e202405426.

29 D. Xiao, Z. Jin, G. Sheng, L. Chen, X. Xiao, T. Shan, J. Wang, R. Navik, J. Xu, L. Zhou, Q.-H. Guo, G. Li, Y. Zhu, J. F. Stoddart and F. Huang, *Nat. Chem.*, 2024, **16**, 1906–1914.

30 F. Yuan, G. Han, C. Chen, X. Fan, S. Xiang and Z. Zhang, *Angew. Chem., Int. Ed.*, 2025, **64**, e202501875.

31 H. Zhou, T. Jiang, K. Fu, X. Guan, S. Guan, B. Liu and H.-L. Jiang, *Angew. Chem., Int. Ed.*, 2025, **64**, e202509174.

32 T. Shan, L. Chen, Z. Guo, D. Xiao, M. Wang, X. Xiao, G. Li and F. Huang, *J. Am. Chem. Soc.*, 2025, **147**, 17477–17485.

33 X.-T. Li, M.-J. Li, Y.-L. Tian, S.-L. Han, L. Cai, H.-C. Ma, Y.-Q. Zhao, G.-J. Chen and Y.-B. Dong, *Nat. Commun.*, 2024, **15**, 8484.

34 F. Yuan, G. Han, C. Chen, X. Fan, S. Xiang and Z. Zhang, *Angew. Chem., Int. Ed.*, 2025, **64**, e202501875.

35 Z. Wang, A. Li, Z. Zhao, T. Zhu, Q. Zhang, Y. Zhang, Y. Tan and W. Z. Yuan, *Adv. Mater.*, 2022, **34**, 2202182.

36 S. Tang, Z. Zhao, J. Chen, T. Yang, Y. Wang, X. Chen, M. Lv and W. Z. Yuan, *Angew. Chem., Int. Ed.*, 2022, **61**, e202117368.

37 L. Gu, H. Shi, L. Bian, M. Gu, K. Ling, X. Wang, H. Ma, S. Cai, W. Ning, L. Fu, H. Wang, S. Wang, Y. Gao, W. Yao, F. Huo, Y. Tao, Z. An, X. Liu and W. Huang, *Nat. Photonics*, 2019, **13**, 406–411.

38 (*a*) CCDC 2414993: Experimental Crystal Structure Determination, 2026, DOI: 10.5517/ccdc.csd.cc2m200r.; (*b*) CCDC 2465520: Experimental Crystal Structure Determination, 2026, DOI: 10.5517/ccdc.csd.cc2nrkxx.